Task-Related Component Analysis Combining Paired Character Decoding for Miniature Asymmetric Visual Evoked Potentials

Yusong Zhou, Banghua Yang, Cuntai Guan, *Fellow, IEEE*

***Abstract*—Brain-computer interface (BCI) technology based on event-related potentials (ERP) of electroencephalography (EEG) is widely used in daily life and medical treatment. However, the research of identifying the miniature and more informative asymmetric visual evoked potentials (aVEPs), which belongs to ERP, needs further exploration. Herein, a task-related component analysis combining paired character decoding (TRCA-PCD) method, which can enhance reproducibility of aVEPs in multiple trials and strengthen the features of different samples, was designed to realize fast decoding of aVEPs. The BCI performance and the influence of repetition times between the TRCA-PCD method, the discriminative canonical pattern matching (DCPM) method and traditional task-related component analysis (TRCA) method were compared using a 32-class aVEPs dataset recorded from 32 subjects. The highest average recognition accuracy and information transfer rate (ITR) of TRCA-PCD after parameter selection were 70.37 ± 2.49% (DCPM: 64.91 ± 2.81%, TRCA: 44.01 ± 3.25%) with the peak value of 97.92% and 28.90 ± 3.83 bits/min (DCPM: 21.29 ± 3.35 bits/min, TRCA: 11.54 ± 2.81 bits/min) with the peak value of 94.55 bits/min respectively. Statistical analysis indicated that the highest average recognition rate could be obtained when the repetition time was six, and the highest ITR could be obtained when the repetition time was one. Overall, the results verified the effectiveness and superiority of TRCA-PCD in recognition of aVEPs and provided a reference for parameter selection. Therefore, the TRCA-PCD method can promote the further application of aVEPs in the BCI speller field.**

***Index Terms*—Brain-computer interfaces (BCI), Event-related potential (ERP), Task-related component analysis (TRCA), Paired character decoding (PCD), Asymmetric visual evoked potentials (aVEPs)**

This work was supported by National Natural Science Foundation of China (No. 61976133), Major scientific and technological innovation projects of Shan Dong Province (No.2019JZZY021010), Shanghai Industrial Collaborative Technology Innovation Project (No. 2021-cyxt1-kj14), Science and technology innovation base project of Shanghai Science and Technology Commission，(No. 19DZ2255200), 111 Project (No. D18003). *(Corresponding author: Banghua Yang.)*

Yusong Zhou and Banghua Yang are with the School of Mechanical Engineering and Automation, Shanghai University, Shanghai 200444, China (e-mail: zhouyusong@shu.edu.cn; yangbanghua@shu.edu.cn).

Cuntai Guan is with the School of Computer Science and Engineering, Nanyang Technological University, Singapore 639798 (e-mail: ctguan@ntu.edu.sg).

I. Introduction

BRAIN-COMPUTER interface (BCI) technology has been developed and gradually applied in clinical practice due to the advances in computer-based biological communication technology [1]. BCI technology is crucial in the new generation of human-computer interaction and human-computer hybrid intelligence. It can establish a direct information communication channel between the human brain and the external environment through the collection, recognition, and transformation of the electrical activities and characteristic signals of the nervous system [2]. ERP recognition technology has steadily developed and has been widely used in BCI research. For instance, Martínez-Cagigal et al. (2017) designed an asynchronous P300-BCI based on the web browser for severely disabled people [3]. Deng et al. also designed a brain-controlled wheelchair system based on steady-state visual evoked potentials (SSVEP) [4]. Moreover, Chen et al. designed a target detection system based on rapid serial visual presentation (RSVP) [5]. Presently, the matrix character flicker paradigm and RSVP paradigm are commonly used to induce ERP. However, both of them require the central visual field of the subjects to feel the strong stimuli flickering screen for robust ERP signal, which can easily lead to visual fatigue, thus limiting multi-task operation [1], [6]. Xu et al. (2018) first proposed a new method for character recognition, which encoded and induced aVEPs through space-code division multiple access (SCDMA) based on the spatial contralateral dominant characteristics of human brain response to stimuli [7].

Traditional BCI systems can recognize the dominant feature of EEG with amplitude larger than 2μV due to non-linear, non-stationary, and strong noise of EEG signal. However, it is a new field that needs further research for the detection of the miniature aVEPs signal, which contains more information [8], [9]. Besides, there is little research on the recognition of aVEPs. Xiao et al. designed and constructed a spatial filter based on the spatial symmetry of EEG. They proposed a discriminative canonical pattern matching (DCPM), which could effectively suppress the common mode noise of left and right hemispheres of the brain and greatly improve the signal-to-noise ratio (SNR) and recognition rate of aVEPs [10-12]. This algorithm is the main algorithm to identify aVEPs at present. Other algorithms, such as stepwise linear discriminant analysis (SWLDA) [13], Bayesian linear discriminant analysis (BLDA) [14], xDAWN [15], and EEGNet [16], have achieved good results in P300 recognition induced by traditional paradigms, but these

algorithms are not as effective as DCPM in recognition of aVEPs [10].

Tanaka et al. proposed a spatial filtering method based on task-related component analysis (TRCA) with advantages in near-infrared spectroscopy (NIRS) data [17], [18]. In terms of SSVEP-BCI, TRCA method is used widely since it can maximize the reproducibility of time-locked activities in the experiment and has good performance in extracting task-related components. In 2017, Nakanishi et al successfully applied this algorithm to SSVEP signal analysis and further proposed an ensemble task-related component analysis method (Ensemble TRCA) which can improve the signal-to-noise ratio (SNR) of the feature signal used for target recognition and further improve the recognition rate of classification and ITR [19]-[21]. Mei et al. applied the TRCA method in controlling the quadcopter, Liu et al used it in the mobile situation, and Zheng et al. used it to decode EEG features in brain switch based on code-modulated visual-evoked potential (c-VEP) [22]-[24]. Zhao et al. designed the steady state peripheral visual evoked potential (SSPVEP) stimulation paradigm to reduce users' visual fatigue using peripheral vision and the Ensemble TRCA algorithm [25]. Tang et al. designed a novel inter TRCA (iTRCA) spatial filter to extract the related components of each flicker in a multifocal SSVEP (mfSSVEP)-based BCI speller [26]. Tanaka et al. maximized both trial-by-trial reproducibility within a single subject and similarity across a group of subjects based on group task-related component analysis (gTRCA) and enhanced ERP evoked and induced responses using cross-correlation task-related component analysis (xTRCA) [27], [28].

In summary, the recognition rate and ITR of aVEPs are lower than traditional P300 and SSVEP. However, the recognition of aVEPs could improve in the future through algorithm improvement. Presently, TRCA has achieved good results in recognition of SSVEP. However, there is little research on TRCA-based algorithm in the field of aVEPs detection. Besides, its recognition ability has not been verified.

The aVEPs are time-locked EEG with two different repetitive stimulation tasks. Therefore, TRCA may have good recognition results for aVEPs since it can maximize the reproducibility of neural data during the task. This study proposed a method to improve the performance of detecting aVEPs signals. First, according to the characteristics of aVEPs, training samples of new structure was used to strengthen the features. Second, the performance was evaluated using a 32-character aVEPs dataset recorded from 32 subjects. The recognition rate and ITR of each subject with different repetition times were calculated based on the Leave-one-out (LOO) Cross-Validation method. Moreover, the influence of repetition times on the recognition results with training was analyzed using Two-way repeated measures ANOVA. The general rules were summarized to provide a reference for parameter selection. This study aimed to demonstrate the efficiency of the TRCA-PCD in the detection of aVEPs and promote further application of aVEPs in the field of BCI speller.

II. Materials and Methods

A. Introduction of aVEPs Dataset

Herein, a miniature aVEPs dataset collected in 2020 WORLD ROBOT COMPETITION-BCI CONTROL BRAIN ROBOT CONTEST consisting of List A and B were used. The data included 32 subjects' continuous EEG data acquisition (14 subjects from List A, 18 subjects from List B). Each person had three blocks with 16 characters of data. Block1 and block3 contained 'M, V, Q, 2, B, W, G, K, P, 5, E, D, O, I, C, 4'. Block2 contained 'S, X, U, Y, R, J, 3, L, H, T, F, A, 6, Z, 1, N'. The data of each character included 6 repeated trials. A single trial had 10 labels (each block had 96 trials, and each subject had 288 trials).

The dataset needs to be obtained after registering and logging in on the Oneuro official website. The dataset link is: https://oneuro.cn/n/competitiondetail/chinabci_2020_erp_with_training/doc1.

B. Experimental Procedure

The main structure of the aVEPs-based character speller is shown in Fig. 1. The background color of the screen was black. Thirty-two white characters were evenly distributed on the screen (4 × 8 matrix). A yellow pentagram visual cue appeared at the beginning of the experiment for 0.8 s directly below the white character, indicating that the subjects were about to pay attention to the stimuli [7]. The subjects needed to quickly move and maintain at the fixation point to the corresponding character. The char label was immediately set on the EEG data when the cue disappeared. The visual stimuli started after 0.2 s. Each visual stimulus had six tiny white dots (clustered within 0.5°) with less than 1 mm diameter. The eccentricity between the cue and the stimuli was 2.1° [10]. The polar angle between the cue and the horizontal axis with the stimuli point as the origin was 135°. SCDMA scheme coding was used for visual stimulation. Parallel channels were formed via the left and right stimulation in space [11]. Herein, the time label representing the character number was named 'char label', and the time label representing the left and right visual stimulation below the character was named 'stimulus label'.

For example, when the character to be watched is '3', first, a yellow pentagram visual cue will firstly appear directly below character '3' on the screen and disappear after holding for 0.8s. Then, after another 0.2 s, a single visual stimulus composed of six tiny white dots will appear on the left below the character '3'. The visual stimulus will disappear after holding for 0.05 s. After that, there is no visual stimulus below the character 3, and this state will last for 0.05 s. The complete process of 0.1s from the appearance to the disappearance of visual stimulus is called 'left - empty'. The stimulus label will record this process as '0'. Similarly, if this process is "right - empty", the stimulus label is set as '1'. Analogously, the stimulus sequence of complete character 3 is 'left - empty - right - empty - right - empty...', Expressed as '011...' with stimulus label. The sequence composed of 10 stimulus labels is called a stimulus sequence. The character '3' is represented as '0110010110', as shown in Table I of Appendix. In particular, the coding feature of 'stimulus label' indicates that each two adjacent stimuli are not repeated, i.e., '10' or '01' appears in pairs. In addition, the char label of character '3' is '121', this means the character '3' is in

the first row of the eighth column on the screen, so the char label can be expressed as '12 (column) + 1 (row)' (The column counts from 5, and 5-12 represents the 1-8 columns of the character on the screen.). Each stimulus sequence will be repeated six times (interval, 0.2 s) to obtain a reliable output. So, each character will contain 60 visual stimuli divided into six groups (10 in each group).

C. Signal Recording and Pre-Processing

Herein, 64 wet electrode EEG acquisition system of Neuroscan Synapps2 was used to collect the data of aVEPs. The EEG cap electrode was installed following the international 10-20 system (Fig. 2). The GND electrode was connected to the AFz electrode, and the REF reference electrode was between the Cz and the CPz electrodes. The experimental paradigm was based on Matlab-2019b. The sampling rate of the original aVEPs data was 1000Hz. It was stored after being processed by a bandpass-filter at 0.1-100Hz and a notch filter at 50Hz.

For data preprocessing, the original data was downsampled to 200Hz. The average value of the left and right mastoid electrodes was then selected for re-reference. The data were filtered at 1-20Hz through Chebyshev filter since the frequency of aVEPs EEG is mainly concentrated within 1-20Hz. It is known that the aVEPs data belongs to visual evoked potentials, and the occipital lobe of the brain is the visual area, which is mainly responsible for vision and image recognition. Therefore, this study selected 21 channels located in the occipital area for analysis to reduce the data dimension further and improve the calculation speed [7], as shown in the blue labeled electrodes in Fig. 2.

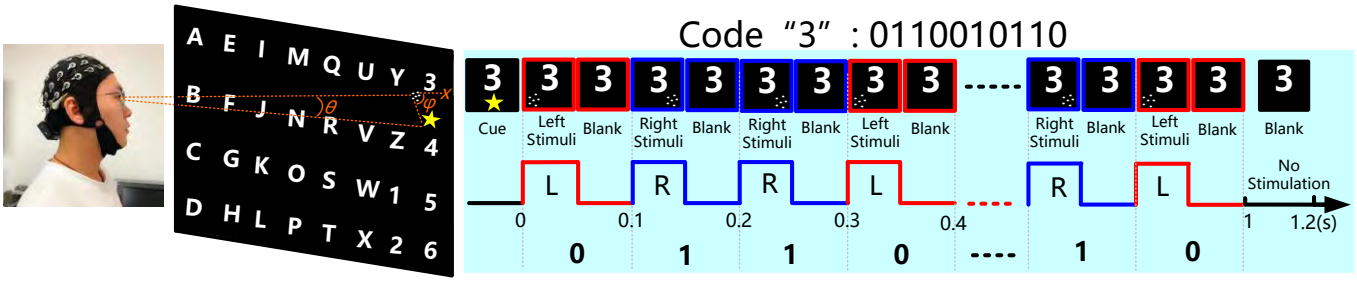

Fig. 1. The paradigm of aVEPs speller. 'θ' and 'φ' represent eccentricity and polar angle, respectively. The blue square represents the stimulus sequence of single-trial of character '3', which was not displayed on the screen during the experiment.

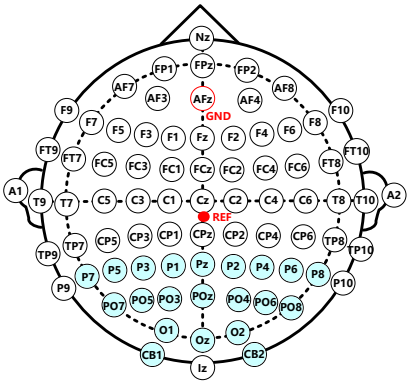

Fig. 2. Channel locations according to the international10-20 system.

D. Discriminative Canonical Pattern Matching (DCPM)

DCPM method is suitable for the single-trial classification of ERP components. It can reduce the training and calibration time and improve the efficiency of ERP-BCI in individual feature recognition. Several studies [10-12] have shown that DCPM has a better classification effect on all ERP features (aVEPs, mVEP, P300, etc.) than other algorithms due to its robustness and generalization classification algorithm.

The main idea of DCPM is to maximize the spatial feature difference between the two types of samples with Discriminative Spatial Patterns (DSP) spatial filter, to reveal the underlying correlation between the filtered training template and the test sample with Canonical Correlation Analysis (CCA) algorithm, to calculate the Pearson correlation between the training template and the test sample with pattern matching. The category corresponding to the maximum correlation coefficient is the test sample category [29]. More details about DCPM can be found in [10-12].

E. Traditional TRCA Method

The overall process of identifying aVEPs using the traditional TRCA algorithm can be divided into three stages: (1) training a spatial filter and a template; (2) calculating a correlation coefficient matrix for testing; (3) decoding computation (Fig. 3 (a)).

Suppose $X_k \in R^{N_c \times N_t \times N_s}, k = 1,2$ are the training sets, where Nc, Nt, Ns and k indicate the number of channels, time points, samples, and label categories, respectively. Suppose X_k can be expressed as $X_k = [x_1, x_2, \ldots, x_i]$, where i represents the index of channels, then a linear model can be expressed as follows [17]:

$$y(t) = \sum_{i=1}^{Nc} w_i x_i(t). \tag{1}$$

w_i indicates the weight matrix, making $y(t)$ consist of the task-related component only. $W_k = [w_1, w_2, ..., w_i]$ can be found via inter-trial covariance maximization. The h-th trial of X_k and the estimated task-related component can be described as $\mathbf{x}^{(h)}(t)$ and $y^{(h)}(t)$, h = 1, 2, ..., Ns. All the covariance between two trials can be summed as follows [19]:

$$\begin{aligned} \sum_{\substack{h_1,h_2 \\ h_1 \neq h_2}}^{Ns} C(h_1,h_2) &= \sum_{\substack{h_1,h_2 \\ h_1 \neq h_2}}^{Ns} \sum_{i_1,i_2=1}^{Nc} w_{i_1} w_{i_2} \\ &\quad \mathrm{Cov}(x_{i_1}^{h_1}(t), x_{i_2}^{h_2}(t)) \\ &= W_k^T S W_k. \end{aligned} \tag{2}$$

where $S = (S_{i_1 i_2})_{1 \le i_1,\, i_2 \le Nc}$ is defined as [19]:

$$S_{i_1 i_2} = \sum_{\substack{h_1, h_2 \\ h_1 \neq h_2}}^{Ns} \mathrm{Cov}(x_{i_1}^{h_1}(t), x_{i_2}^{h_2}(t)). \tag{3}$$

The normalization constraint of $y(t)$ can be described as follows [17]:

$$\begin{aligned} \mathrm{Var}(y(t)) &= \sum_{i_1, i_2 = 1}^{Nc} w_{i_1} w_{i_2} \mathrm{Cov}(x_{i_2}(t), x_{i_2}(t)). \\ &= W_k{}^T Q W_k \\ &= 1. \end{aligned} \tag{4}$$

The optimal weight vector $\hat{W}_k$ can be obtained based on Rayleigh-Ritz theory as follows [17]:

$$\hat{W}_k = \arg\max_{W_k} \frac{W_k{}^T S W_k}{W_k{}^T Q W_k}. \tag{5}$$

$\hat{W}_k$ indicates the eigenvector corresponding to the eigenvalues of $Q^{-1}S$ in a descending order.

The correlation coefficient between the data of the m-th label in the single-trial testing data (10 labels) $Y \in R^{Nc \times Nt}$ and averaged training data across trials for k-th label category $\overline{X}_k \in R^{Nc \times Nt}$ can be calculated as follows [19]:

$$r_k^{(m)} = \rho(Y^T W_k, \overline{X}_k{}^T W_k). \tag{6}$$

$\rho(\boldsymbol{a}, \boldsymbol{b})$ indicates the two-dimensional correlation analysis between $\boldsymbol{a}$ and $\boldsymbol{b}$, k=1, 2, m=1, 2, …, 10.

Then the predicted code of the m-th label in Y is

$$\hat{k} = \arg\max_k r_k^{(m)}. \tag{7}$$

Finally, a 10-bit character can be encoded and compared with the code list in Table I of Appendix. The recognition result can be output only when it is completely matched.

F. TRCA-PCD Method

1) The Training and Testing DATA

Different from the traditional TRCA algorithm, X_1 in the task-related component analysis combining paired character decoding (TRCA-PCD) method represents all training data with label categories of '01' and '00' instead of '0', similarly, X_2 represents '10' and '11' instead of '1'. This is due to ERP having significant nonlinear reorganization of ongoing oscillations under weak stimulation [7], [30]. So, the aVEPs pattern would influence the following one or even more. Specifically, label 0 had at least two ERP patterns corresponding to sequences '00', '01', respectively, while label 1 corresponding to '10', '11'. Therefore, the m-th label in testing data Y should also be set to the corresponding data length during the test, so as to ensure the same dimension as the training data.

2) Parameter Selection

Suppose the eigenvalues of $Q^{-1}S$ in the formula (5) are λ_1, λ_2, …, λ_{Nc}(sorted in descending order). The smallest value of p should satisfy:

$$\frac{\sum_{j=1}^{p} \lambda_j}{\sum_{j=1}^{Nc} \lambda_j} \geq 0.9. \tag{8}$$

where λ_j, Nc and p indicate the j-th eigenvalues of $Q^{-1}S$, the number of total eigenvalues of $Q^{-1}S$ and the first p eigenvalues of $Q^{-1}S$, respectively. This means 90% of the variance was retained. So, the new spatial filter can be written as W_k^p. The idea of principal component analysis (PCA) is used here.

3) Calculation of Decoding

After the calculation of formula (6), suppose the repetition times are n, $(r_k^{(m)})_j$ represents the correlation coefficient between the m-th label in the j-th trial of testing data and the averaged training data across trials for k-th label category, and the final correlation coefficient $r^{(m)}$ can be calculated as follows:

$$\bar{r}^{(m)} = \frac{1}{n} \sum_{j=1}^{n} ((r_2^{(m)})_j - (r_1^{(m)})_j). \tag{9}$$

It should be noted that during the decoding process, starting from $r^{(1)}$, the step size is two values, and the two adjacent values are read in turn. The first value is recorded as "10" if greater than the second value; else, "01". The code can be finally forecasted by follows:

$$\mathrm{code}^{(l,l+1)} = \begin{cases} '10', r^{(l)} - r^{(l+1)} > 0 \\ '01', r^{(l)} - r^{(l+1)} < 0 \end{cases}, l = 1, 3, ..., 9. \tag{10}$$

This decoding method can improve the recognition rate to a certain extent compared to using a single correlation coefficient for discrimination. The implementation of the TRCA-PCD method is shown in Fig. 3 (b).

4) The Recognition Principle of TRCA-PCD

The principle of using TRCA-PCD to identify aVEPs is shown in Fig. 4. The difference between channel 'PO7' and channel 'PO8' became obvious after processing of averaging due to the significant effects of aVEPs (Fig. 4 (a) and (c)) [8]. The brain topographic maps also show the significant differences between the two stimuli responses in the occipital region. Therefore, the recognition of aVEPs can be realized if the characteristics of two ERP patterns are found. TRCA-PCD mainly extracts the most relevant components in similar tasks.

The relevant components of the two stimulus sequences are found after W_1 and W_2 filtering and being arranged from large to small based on the correlation (Fig. 4 (b) and (d)). The main components of the two stimuli have opposite trends. Several most relevant components are selected as the feature templates of aVEPs to accurately recognize aVEPs and reduce the dimension. The correlations between the test data and the feature templates of the two stimulus sequences are calculated via the Pearson correlation coefficient. The larger the correlation coefficient is, the closer the test data are to the feature template, thus achieving the final recognition.

The essence of TRCA-PCD method to outperform the traditional TRCA is that the sample features can be strengthened when using paired samples for training and decoding, thereby improving the recognition accuracy.

G. Evaluation of Algorithms

1) Evaluation Criterion

The performance of the TRCA-PCD based method was analyzed by simulating an online test on the dataset. The recognition accuracy and ITR of different subjects and numbers of testing trials were calculated based on the LOO

method with block as the unit. One block of data was left for each test. The rest of the data was used for training until all blocks were tested. Similarly, the data stream of the test was provided by simulating online. A new packet was obtained based on the required repetition times by calling the data reading method every time. The packet recorded the label information received in the reading process and the length of the aVEPs signal used. Packets in the same block were sent in chronological order. The block end flag in the last packet was set to 1 after all data in a block were sent. The program termination flag was set to 1 when all the experimental data was sent.

The recognition accuracy and ITR can be used as the evaluation criteria. ITR can be calculated as follows [31]:

$$\mathrm{ITR} = (\log_2 N + P\log_2 P + (1-P)\log_2 \frac{1-P}{N-1}) \times (\frac{60}{T}). \quad (11)$$

N indicates the number of characters in each block, P represents the recognition accuracy, and T shows the average test time. ITR can be calculated in bits/min. Length of EEG data obtained from the beginning of character stimulation to the time when the algorithm is called can be used as the time length of the trial. The average time length of repetition times is the average trial time T to calculate ITR. The recognition accuracy can be calculated based on the consistency of the decoding result and the actual data code.

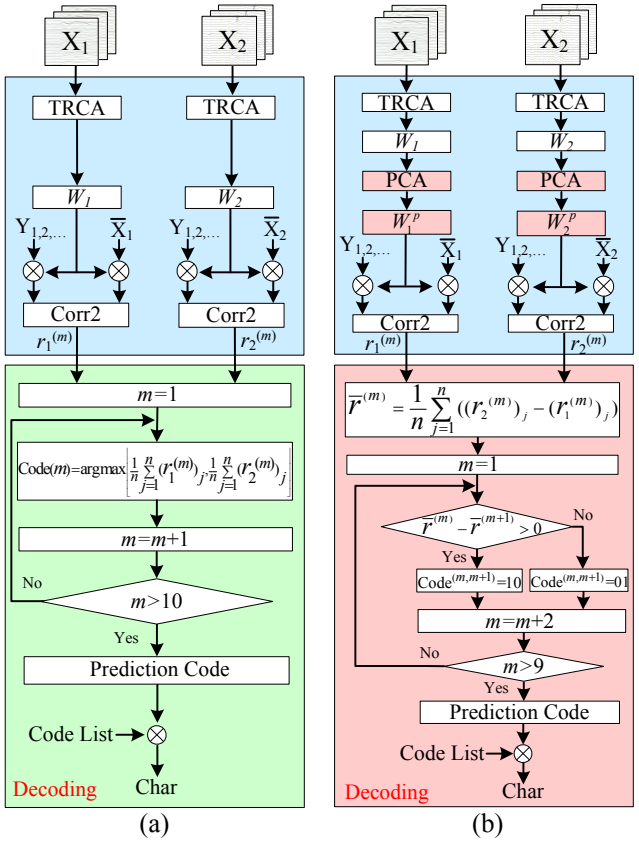

Fig. 3. Diagrams of the TRCA (a) and TRCA-PCD (b) methods. The green box in (a) and the red part in (b) represent the differences between the two algorithms, respectively.

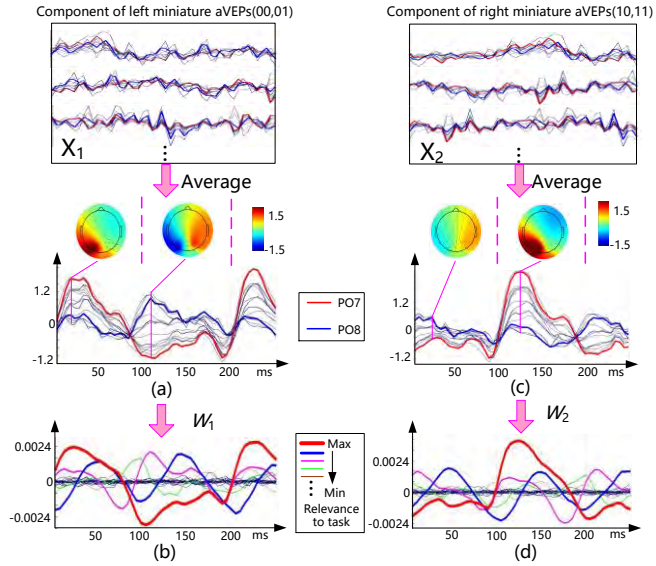

Fig. 4. Identification principle of TRCA-PCD. X_1 contains the component of left miniature aVEPs ('00','01'), X_2 contains the component of right miniature aVEPs ('10','11'). (a) The averaging of X_1. (b) Related components of left miniature aVEPs. (c) The averaging of X_2. (d) Related components of right miniature aVEPs. The red and blue lines in (a) and (c) represent channel PO7 and PO8, respectively. Lines from thick to thin in (b) and (d) indicate the correlations from large to small. The red lines in (b) and (d) represent the largest correlation component, and the blue lines represent the second-largest correlation component, etc.

2) *Statistical Method*

SPSS 26.0 statistical software was used to assess the effect of the different methods and repetition times on recognition accuracy and ITR. Shapirov-Wilk test was used to evaluate whether the recognition accuracy and ITR conformed to normal distribution. Two-way repeated measures ANOVA was used to judge the impact of different algorithms on accuracy and ITR with the change of repetition times. All significant levels were selected as $\alpha = 0.05$ to obtain the general rule of the algorithms in processing aVEPs. The Greenhouse-Geisser method was used to correct Mauchly's Test of Sphericity. The Bonferroni correction was adopted for multiple comparisons of methods and repetition times.

3) *Selection of data length*

According to the reference [30], the significant feature of aVEPs will appear at 200-300 ms after stimulation. The length of single data packet read by the simulated online test system is 50ms (10 sample points), so the data lengths which could be obtained between 200-300 ms are 200 ms, 250 ms and 300 ms. In order to further verify which data length would achieve the best performance, the experiments of 200ms, 250ms and 300ms data lengths could be used for comparative analysis.

III. RESULTS

A. *Target Identification Performance*

Fig. 5 shows the highest average recognition results estimated by a LOO method across 32 subjects with different data lengths (the segmented window sizes were 200ms, 250ms and 300ms). The green, blue and red bar graphs represent the recognition results of TRCA, DCPM and TRCA-PCD,

This article has been accepted for publication in a future issue of this journal, but has not been fully edited. Content may change prior to final publication. Citation information: DOI 10.1109/TNSRE.2022.3175307, IEEE Transactions on Neural Systems and Rehabilitation Engineering

respectively.

The accuracy of all subjects increased with the increasing of repetition times. The ITR decreased with the increasing of repetition times while adopting TRCA-PCD and DCPM methods. But the highest ITR result with the traditional TRCA method could be achieved when the repetition time was 3.

The highest averaged accuracy rate of TRCA-PCD (70.37 ± 2.49%, data length = 300 ms, repetition time = 6) was 5.46% higher than that of DCPM (64.91 ± 2.81%, data length = 300 ms, repetition time = 6) and 26.26% higher than that of TRCA (44.01 ± 3.25%, data length = 300 ms, repetition time = 6).

The fastest average ITR of TRCA-PCD (28.90 ± 3.83 bits/min, data length = 250 ms, repetition time = 1) was 7.61 bits/min faster than that of DCPM (21.29 ± 3.35 bits/min, data length = 300 ms, repetition time = 1) and 17.36 bits/min faster than that of TRCA (11.54 ± 2.81 bits/min, data length = 250 ms, repetition time = 3). More detailed results are shown in Table II in Supporting Document.

The comparison of the three methods indicates that the TRCA-PCD method outperforms the DCPM and traditional TRCA method. And the TRCA-PCD method helps to achieve the best performance regardless of data length.

B. Statistical Analysis Results

The accuracy results showed that the interactions between methods and repetition times were statistically significant (data length = 200ms, F (5.99, 185.64) = 19.74, $p < 0.001$; data length = 250ms, F (5.79, 179.41) = 6.73, $p < 0.001$; data length = 300ms, F (5.08, 157.35) = 4.73, $p < 0.001$). The ITR results showed that the interactions between methods and repetition times were statistically significant (data length = 200ms, F (2.24, 69.30) = 14.07, $p < 0.001$; data length = 250ms, F (2.71, 83.84) = 15.53, $p < 0.001$; data length = 300ms, F (2.40, 74.24) = 14.72, $p < 0.001$).

When the interaction is meaningful, it's not significant to analyze the main effect alone. It's necessary to analyze the difference of accuracy and ITR with different methods at different repetition times one by one, that is, the individual effect of internal factors in each subject. The detailed results are shown in Table III in Supporting Document.

When the data length was 250 ms in the ITR result, there had significant differences between TRCA-PCD and DCPM, TRCA-PCD and TRCA (repetition time = 4, 5, 6, $p < 0.01$), but there had no significant differences between DCPM and TRCA (repetition time = 4, 5, 6, $p > 0.05$). In all other situations, the simple effects of the three methods were statistically significant ($p < 0.01$) to accuracy and ITR with the change of repetition times.

When the data length was 200 ms and 250 ms, the simple effects of repetition times were not statistically significant ($p > 0.05$) to ITR with the TRCA method. In all other situations, the simple effects of repetition times were statistically significant ($p < 0.05$) to accuracy and ITR with different methods.

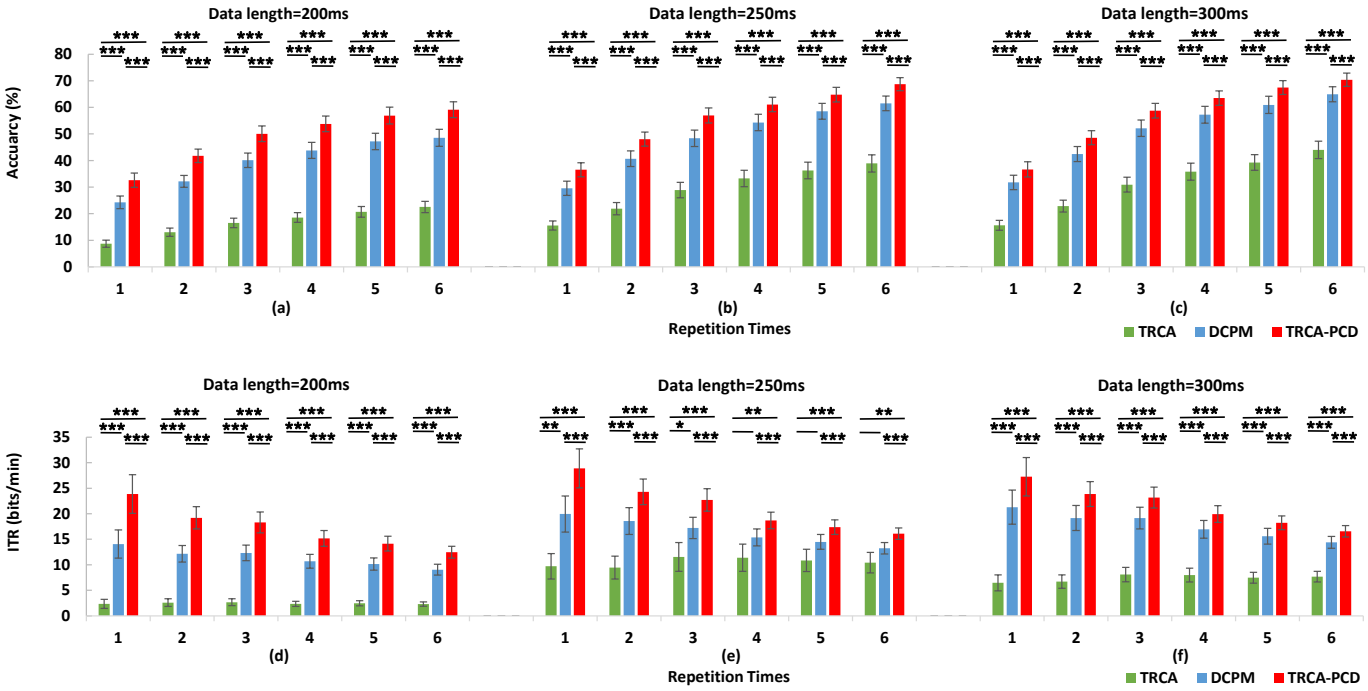

Fig. 5. Optimal averaged recognition accuracy and ITR of the three methods with different repetition times for all subjects. (a) The accuracy results with 200 ms' data. (b) The accuracy results with 250 ms' data. (c) The accuracy results with 300 ms' data. (d) The ITR results with 200 ms' data. (e) The ITR results with 250 ms' data. (f) The ITR results with 300 ms' data. The error bars indicate standard errors. The asterisks in all subfigures indicate significant differences between the three methods obtained by one-way repeated measures ANOVAs (* $p < 0.05$, ** $p < 0.01$, *** $p < 0.001$).

IV. Discussions

Presently, non-invasive brain-computer interaction technology is widely used because it is simple and fast but less costly. Besides, researchers have provided some improvements of software and hardware to achieve a good human-machine interaction experience. For instance, EEG acquisition equipment with semi-dry and dry electrodes can save the time of injecting conductive paste. Moreover,

This article has been accepted for publication in a future issue of this journal, but has not been fully edited. Content may change prior to final publication. Citation information: DOI 10.1109/TNSRE.2022.3175307, IEEE Transactions on Neural Systems and Rehabilitation Engineering

washing the hair will not be required after the experiment, thus improving the efficiency of the experiment [32, 33]. The wireless signal transmission mode is more convenient for EEG data acquisition in motion scenes [34-36]. The human-machine interface with mild weak stimulation can greatly save visual resources and reduce fatigue and other discomforts [8, 37]. The aVEPs are weak visual stimulation-evoked potentials, which were proposed in 2018. It will be widely used in the BCI speller field with a good application prospect after improving recognition and ITR. Although the TRCA-based algorithm has rapidly developed and was applied in the SSVEP recognition field in 2017, it is rarely used in other evoked EEG fields, such as P300 and aVEPs. To find new applications, an improved TRCA algorithm is used here to recognize aVEPs. The results showed that the proposed TRCA-PCD algorithm could efficiently recognize aVEPs, and the averaged accuracy of some subjects (subject 11, subject 26) could even reach 97.92%. Therefore, this study can promote further application of aVEPs.

Herein, data of three blocks of each subject were cross-verified through online simulation. The data transmission and processing were consistent with the real online test, indicating that the results were consistent with the online results. This conclusion has been verified in the 2020 WORLD ROBOT COMPETITION-BCI CONTROL BRAIN ROBOT CONTEST. Block1 and block3 were the EEG data of the same group character, and block2 was the EEG data of another group character. The experimental results indicated that the cross-validation results were stable. Moreover, it still had a high recognition rate when using one group of character data for training to recognize another group of character data. Therefore, the proposed TRCA-PCD method is featured by good robustness and migration recognition ability.

The form of training samples and spatial filter were created after drawing upon the idea of references [7] and [30]. This is different from Wong et al (2020). The key idea of them is to use the target stimulus and the neighboring stimuli to construct the spatial filter W_k [38]. It is worth noting that the so-called 'neighboring stimuli' are due to their nearby flickering frequencies. This means that the stimuli are not necessarily continuous in space. At the same time, each stimulus sample is trained using an integral trial as one unit. Fig. 6 shows the generation of spatial filter W_k from learning across multi stimulus. However, the spatial filter of the TRCA-PCD proposed by us is obtained from the samples dominated by a single type of stimulus. The spatial filter W_1 is obtained from the left stimulus dominated samples ('00', '01'), and the spatial filter W_2 is obtained from the right stimulus dominated samples ('10', '11'). At the same time, the TRCA-PCD algorithm decomposes the single trial to obtain the training samples, and combines the recognition results to decode the characters. Fig. 7 shows the generation of spatial filter from the TRCA-PCD method.

The essential reason why the TRCA-PCD learns through continuous stimuli is that the previous stimulus will affect the subsequent adjacent stimuli. Due to the fact that characters are binary coded, '0' can only be followed by '0' or '1', and '1' can only be followed by '0' or '1'. This seems similar to learning from two stimuli, but in fact it is not. Without learning from continuous stimuli, the TRCA-PCD method cannot learn the effective data features because it is out of the influence range of a single stimulus.

In statistical analysis, it was considered that the values with student residuals exceeding ± 3 are outliers, and the outliers were reported in Table IV in Supporting Document. The results show that almost all ACC and ITR outliers were generated by subject 17. We recalculated the results of abnormal values, and the results were consistent. It was confirmed that these abnormal values belong to real outliers. This shows that subject 17 could induce aVEPs with obvious characteristics, which exists in the actual EEG experiment. It is necessary to consider the role of this kind of subject in the overall population, so these outliers were still enrolled in the statistical calculation.

According to the recognition accuracy and ITR of the methods for all subjects in Fig. 5, it can be seen that in the online test with training, the offline training can find out the repetition times needed under the condition of the best recognition result, so as to optimize the program and improve the average recognition rate and ITR in the online test. However, in the online test without training, due to the lack of training data, the optimal parameters can not be determined. The general rule can be summarized through the statistics of the results in this paper: In the pursuit of the highest recognition accuracy, the number of testing trials can be set to 6; in the pursuit of the highest ITR, the number of testing trials can be set to 1.

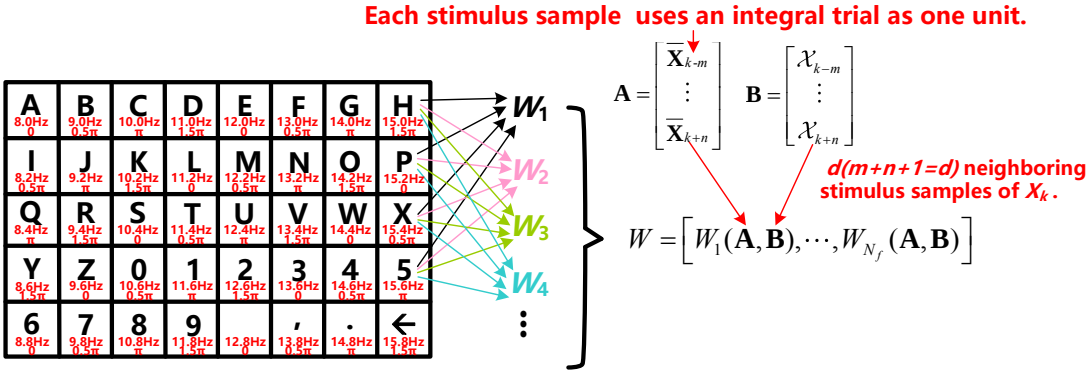

Fig. 6. Generation of spatial filter from learning across multi stimulus in the ms-eTRCA method. $\bar{X}_k$ is the average of the SSVEP data across a number of training trials for the k-th visual stimulus. $\mathcal{X}_k$ is the transpose of all trials' assemble of X_k^T. **A** consists of d neighboring stimulus samples of $\bar{X}_k$, **B** consists of d $\mathcal{X}_k$. The final W consists of W_1 to W_{Nf}.

This article has been accepted for publication in a future issue of this journal, but has not been fully edited. Content may change prior to final publication. Citation information: DOI 10.1109/TNSRE.2022.3175307, IEEE Transactions on Neural Systems and Rehabilitation Engineering

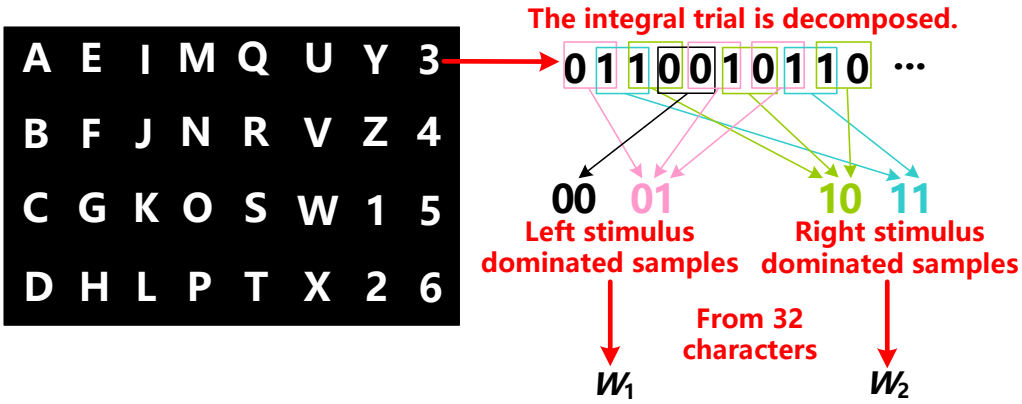

Fig. 7. Generation of spatial filter from the TRCA-PCD method. The W_1 is generated by the left stimulus dominated samples from all characters, and the W_2 is generated by the right stimulus dominated samples from all characters. These samples are all decomposed from the complete trials.

In this paper, the repetition times refer to the number of times the algorithm needs to repeatedly obtain the character data to recognize a character in an online simulation test. This is consistent with the description in reference [7]. For an online system, when the repetition times of obtaining character data increase, the calculation time becomes longer, which will reduce the value of ITR. Although the recognition accuracy is improved, on the whole, ITR will eventually show a downward trend since the calculation time has a greater impact on ITR.

It is undeniable that there are some shortcomings in this study. First, the accuracy increased with repetition times, but there were only six repetition times in the dataset for each subject. Therefore, more repetition times are needed to assess whether and when the accuracy rate tends to converge. Second, combined with the statistical analysis results, the aVEPs recognition accuracy based on TRCA-PCD was negatively correlated with ITR. However, the algorithm should have achieved the highest accuracy and ITR at the same time. In addition, the impact of different number of training sets on the TRCA-PCD method has not been studied. Further studies are in need to explore the above problems.

V. Conclusion

This study designed the TRCA-PCD algorithm to assess the recognition of aVEPs based on the data acquired from 32 subjects. The performance of TRCA-PCD was evaluated through recognition accuracy, ITR indicators, and statistical analysis. The results show that the TRCA-PCD algorithm has better recognition performance in recognition of aVEPs than DCPM and TRCA. In any case, this study provides a solid basis for the research of recognition of aVEPs in the future.

Appendix

TABLE I
Character Label and Code

Char/LBL	Code	Char/LBL	Code	Char/LBL	Code	Char/LBL	Code
A/51	0110100101	I/71	1001011010	Q/91	1010010101	Y/111	0110101001
B/52	0110011001	J/72	0101011001	R/92	0101010110	Z/112	1010101001
C/53	0110010101	K/73	0101100110	S/93	1001100101	1/113	1010011010
D/54	0101101010	L/74	1010010110	T/94	0110011010	2/114	1010101010
E/61	1001100110	M/81	1001101001	U/101	1010100101	3/121	0110010110
F/62	1001011001	N/82	0110100110	V/102	1001010110	4/122	1001101010
G/63	0101100101	O/83	1010100110	W/103	1001010101	5/123	0101010101
H/64	1010011001	P/84	0101101001	X/104	0101011010	6/124	0110101010

References

[1] X. Chen *et al*., "High-speed spelling with a noninvasive brain–computer interface," *Proc. Natl. Acad. Sci.*, vol. 112, no. 44, pp. E6058-E6067, Oct. 2015.

[2] J. R. Wolpaw, E. W. Wolpaw. *Brain-computer interface principles and practice*. Oxford, NY, USA: OUP, 2012, pp. 1-496.

[3] V. Martínez-Cagigal, J. Gomez-Pilar, D. Álvarez and R. Hornero, "An Asynchronous P300-Based Brain-Computer Interface Web Browser for Severely Disabled People," *IEEE Trans. Neural Syst. Rehabil. Eng.*, vol. 25, no. 8, pp. 1332-1342, Aug. 2017.

[4] X. Deng, Z. L. Yu, C. Lin, Z. Gu and Y. Li, "A Bayesian Shared Control Approach for Wheelchair Robot with Brain Machine Interface," *IEEE Trans. Neural Syst. Rehabil. Eng.*, vol. 28, no. 1, pp. 328-338, Jan. 2020.

[5] J. Chen *et al*., "Feature Selection of Deep Learning Models for EEG-Based RSVP Target Detection," *IEICE Trans. Inf. Syst.*, vol. E102-D, no. 4, pp. 836-844, Apr. 2019.

[6] Farwell L. A. and Donchin E. "Talking off the top of your head: toward a mental prosthesis utilizing event-related brain potentials," *Electroencephalogr. Clin. Neurophysiol.*, vol. 70, no. 6, pp.510-523, Dec. 1988.

[7] M. Xu *et al*., "A Brain–Computer Interface Based on Miniature-Event-Related Potentials Induced by Very Small Lateral Visual

Stimuli," *IEEE Trans. Biomed. Eng.*, vol. 65, no. 5, pp. 1166-1175, May 2018.

[8] L. D. Blumhardt *et al*., "The asymmetrical visual evoked potential to pattern reversal in one half field and its significance for the analysis of visual field defects," *Brit. J. Ophthalmology*, vol. 61, no. 7, pp. 454–461, Jul. 1977.

[9] H. Strasburger *et al*., "Peripheral vision and pattern recognition: A review," *J. Vis.*, vol. 11, no. 5, pp. 13-13, Dec. 2011.

[10] X. Xiao *et al*., "Discriminative Canonical Pattern Matching for Single-Trial Classification of ERP Components," *IEEE Trans. Biomed. Eng.*, vol. 67, no. 8, pp. 2266-2275, Aug. 2020.

[11] M. Xu *et al*., "Effects of stimuli position on the classification of miniature asymmetric VEPs for brain-computer interfaces," in *Proc. 41st Ann. Int. Conf. IEEE Eng. Med. Biol. Soc. (EMBC)*, Berlin, Germany, 2019, pp. 5956-5959.

[12] L. Yue *et al*., "A brain-computer interface based on high-frequency steady-state asymmetric visual evoked potentials*," in *Proc. 42nd Ann. Int. Conf. IEEE Eng. Med. Biol. Soc. (EMBC)*, Montreal, QC, Canada, 2020, pp. 3090-3093.

[13] D. J. Krusienski *et al*., "Toward enhanced P300 speller performance," *J. Neurosci. Methods*, vol. 167, no. 1, pp. 15–21, Jan. 2008.

[14] U. Hoffmann *et al*., "An efficient P300-based brain-computer interface for disabled subjects," *J. Neural Eng.*, vol. 167, no. 1, pp. 115–125, 2008.

[15] B. Rivet *et al*., "xDAWN algorithm to enhance evoked potentials: Application to brain-computer interface," *IEEE Trans. Biomed. Eng*., vol. 56, no. 8, pp. 2035–2043, Aug. 2009.

[16] V. J. Lawhern *et al.*, "EEGNet: A compact convolutional neural network for EEG-based brain-computer interfaces," *J. Neural Eng.*, vol. 15, no. 5, pp. 056013.1-056013.17, Oct. 2018.

[17] H. Takana *et al.*, "Task-related component analysis for functional neuroimaging and application to near-infrared spectroscopy data," *NeuroImage*, vol. 64, pp. 308–327, Jan. 2013.

[18] H. Takana *et al*., "Task-related oxygenation and cerebral blood volume changes estimated form NIRS signals in motor and cognitive tasks," *NeuroImage*, vol. 94, pp. 107–119, Jul. 2014.

[19] M. Nakanishi *et al*., "Enhancing Detection of SSVEPs for a High-Speed Brain Speller Using Task-Related Component Analysis," *IEEE Trans. Biomed. Eng.*, vol. 65, no. 1, pp. 104-112, Jan. 2018.

[20] G. R. Burkitt, R. B. Silberstein, P. J. Cadusch, and A. W. Wood, "Steady-state visual evoked potentials and travelling waves," *Clin. Neurophysiol.*, vol. 111, no. 2, pp. 246-258, Feb. 2000.

[21] J. M. Ales and A. M. Norcia, "Assessing direction-specific adaptation using the steady-state visual evoked potential: Results from EEG source imaging," *J. Vis.*, vol. 9, no. 7, pp. 8-8, Jul. 2009.

[22] J. Mei *et al.*, "Using SSVEP-BCI to Continuous Control a Quadcopter with 4-DOF Motions*," in *Proc. EMBC*, Montreal, QC, Canada, 2020, pp. 4745-4748.

[23] A. Liu *et al.*, "Muscle Artifact Removal Toward Mobile SSVEP-Based BCI: A Comparative Study," *IEEE Trans. Instrum. Meas.*, vol. 70, pp. 1-12, Jun. 2021, Art no. 4005512.

[24] L. Zheng, Y. Wang, W. Pei and H. Chen, "A Fast Brain Switch Based on Multi-Class Code-Modulated VEPs *," in *Proc.* in *Proc. 41st Ann. Int. Conf. IEEE Eng. Med. Biol. Soc. (EMBC)*, Berlin, Germany, 2019, pp. 3058-3061.

[25] X. Zhao, Z. Wang, M. Zhang, and H. Hu, "A comfortable steady state visual evoked potential stimulation paradigm using peripheral vision," *J. Neural Eng.*, vol. 18, no. 5, 2021, Art. no.056021.

[26] J. Tang *et al*., "A Brain-Computer Interface Based on Multifocal SSVEPs Detected by Inter-Task-Related Component Analysis," *IEEE Access*, vol. 8, pp. 138539-138550, Jul. 2020.

[27] H. Tanaka and M. Miyakoshi, "Cross-correlation task-related component analysis (xTRCA) for enhancing evoked and induced responses of event-related potentials," *Neuroimage*, vol. 197, pp. 177–190, Aug. 2019.

[28] H. Tanaka, "Group task-related component analysis (gTRCA): a multivariate method for inter-trial reproducibility and inter-subject similarity maximization for EEG data analysis," *Sci. Rep*., vol. 10, no. 84, pp. 1-17, Jan. 2020.

[29] X. Liao *et al.*, "Combining spatial filters for the classification of singletrial EEG in a finger movement task," *IEEE Trans. Biomed. Eng.*, vol. 54, no. 5, pp. 821–831, May. 2007.

[30] M. Xu *et al.*, "Use of a steady-state baseline to address evoked vs. oscillation models of visual evoked potential origin," *Neuroimage*, vol. 134, pp. 204–212, Jul. 2016.

[31] M. Nakanishi *et al*., "A high-speed brain speller using steady-state visual evoked potentials," *Int. J. Neural Syst.*, vol. 24, no. 6, Sep. 2014, Art. no. 1450019.

[32] J. R. Wolpaw *et al*., "Brain-computer interface technology: A review of the first international meeting," *IEEE Trans. Rehabil. Eng*., vol. 8, no. 2, pp. 164–173, Jun. 2000.

[33] S. L. Kappel *et al*., "Dry-Contact Electrode Ear-EEG". *IEEE Trans. Biomed. Eng.*, vol. 66, no. 1, pp. 150-158, Jan. 2019.

[34] P. Paulo *et al*., "Alginate-based hydrogels as an alternative to electrolytic gels for rapid EEG monitoring and easy cleaning procedures," *Sensor. Acutat. B*, vol. 247, no. 1, pp.273-283, Jan. 2017.

[35] Y. M. Chi, T. Jung and G. Cauwenberghs, "Dry-Contact and Noncontact Biopotential Electrodes: Methodological Review," *IEEE Rev. Biomed. Eng.*, vol. 3, pp. 106-119, Oct. 2010.

[36] Y. Chen, B. Lin and J. Pan, "Novel Noncontact Dry Electrode with Adaptive Mechanical Design for Measuring EEG in a Hairy Site," *IEEE Trans. Instrum. Meas.*, vol. 64, no. 12, pp. 3361-3368, Dec. 2015.

[37] D. Kapgate, D. Kalbande, and U. Shrawankar, "An optimized facial stimuli paradigm for hybrid SSVEP+P300 brain computer interface," *J. Neurosurg. Sci.*, vol. 59, pp. 114-122, Jan. 2020.

[38] C. M. Wong *et al*. "Learning across multi-stimulus enhances target recognition methods in SSVEP-based BCIs，" *J. Neural Eng.*, vol. 17, no. 1, pp. 016026.1-016026.18, Jan. 2020.